Synthesis and Microstructural Evolution of Amorphous/Nanocrystalline Steel Coatings by Different Thermal-Spray Processes

V. Varadaraajan, Ramesh K. Guduru, and P.S. Mohanty

Amorphous/nanocrystalline coatings are useful in high strength and wear-resistant applications. In the present study, the microstructural evolution of a nanocrystalline high performance steel coatings developed by different spray processes along with a novel "hybrid thermal spray" technique was studied. The hybrid-spray process combines arc and high-velocity oxy-fuel (HVOF) techniques, in which the molten metal at the arcing tip is atomized and rapidly propelled toward the substrate by HVOF jet. This so-called hybrid concept offers the benefits of productivity of electric arc spray combined with improved coating densities of HVOF. The microstructural characterization of the hybrid-spray coatings was performed by x-ray diffraction, electron microscopy, and differential scanning calorimetry, and then compared with coatings of the similar material developed by plasma-, HVOF-, and arc-spray processes individually. The HVOF- and plasma-spray coatings showed amorphous structures with very fine nanocrystals embedded, whereas hybrid- and arc-spray techniques yielded completely crystalline coatings with grain size in the range of several nanometers. The final microstructures in different spray processes could be attributed to the precursor materials employed, process temperatures, and cooling rates during the deposition process.

1. Introduction

In recent years, considerable efforts have been directed toward developing coatings containing amorphous/nanocrystalline structures because of their superior properties that go far beyond the capabilities of usual microcrystalline structured coatings (Ref 1–12). Among the existing coating manufacturing techniques, thermal spray has gained a significant share in developing these coatings (Ref 13–21). There are two possible paradigms that can explain the occurrence of amorphous/nanocrystallinity in thermal sprayed coatings. One of the paradigms is the creation of amorphous/nanoscale structure while the other is the preservation of amorphous/nanoscale structures. Under the creation paradigm; the material melts completely during spray and then undergoes rapid quenching, followed by copious nucleation. Retaining of amorphous structure with this approach is limited, especially when the deposit thickness goes beyond a few hundreds of microns. When successive layers are deposited, the earlier layers may completely lose their amorphous/nanoscale structures due to crystallization or grain growth and coarsening from the heat input with the new layers. Under the preservation paradigm, the amorphous/nanoscale structure exists in the feedstock powders itself. If the amorphous structure of the powders is thermally stable, then retaining amorphous/nanoscale structures in the coatings may not be difficult with successive deposition of several layers and heat input. Recently it has been demonstrated that thick coatings (>several hundred microns) can be made while preserving considerable amount of amorphous/nanoscale structure (Ref 5, 13). These coatings have been developed from complex precursor alloys of iron, and the alloy compositions were conceived from the basic principles of metallic glass formation. Several alloys under the trade name of "nanosteel" and "liquid metal" are now commercially available in wire as well as powder form for fabricating coatings using thermal spray processes. Since the phase evolution in these coatings is dependent on the thermal history of the deposit and precursor materials, the spray process employed to manufacture them also has tremendous influence on the microstructural evolution.

Among the existing variants of thermal-spray technologies, high-velocity oxy-fuel (HVOF) spray represents a major development. The HVOF gun results in hypersonic flame gas velocity, and powder particles attain high heat along with high velocities, which permits particle flattening upon striking the substrate and result in dense coatings. HVOF sprayed metallic coatings often have properties superior to those of plasma/arc-sprayed coatings. Processing of amorphous/nanocrystalline coatings by HVOF technique has also been reported in the literature

V. Varadaraajan, Ramesh K. Guduru, and **P.S. Mohanty**, Department of Mechanical Engineering, University of Michigan, 4901 Evergreen Road, Dearborn, MI 48128. Contact e-mail: rameshkumarg5@yahoo.com.

(Ref 14–20). For conventional metallic coatings, the twin-wire arc-spray gun is a widely used. The main attractions are the low cost and the operational simplicity. During the process, electric arc melts the wires, and the molten metal is atomized by a continuous flow of either high-velocity compressed air or non-oxidizing gases, such as nitrogen (N_2), or argon (Ar). Coatings formed using electric arc-spray gun are relatively porous, but deposition rates are much higher compared to the HVOF process. Arc-spray process has been employed to manufacture amorphous/nanocrystalline coatings in the references (Ref 17–19). The plasma process is mainly used for ceramic or cermets because of the high temperature requirement; however, there exists a vast literature on techniques employing plasma spray to develop amorphous/nanocrystalline coatings (Ref 20, 21).

Recently, we developed a process called "hybrid-spray process" in our laboratory that combines electric arc and HVOF spraying techniques (Ref 22–24). In this process, molten metal at the arc is atomized and rapidly propelled toward the substrate by a HVOF jet (see Fig. 1). This so-called "hybrid" concept aims at exploiting the benefits of both the processes. The process offers all the benefits of wire stock and productivity of electric arc spray combined with noticeably improved coating density of HVOF. Besides, producing high throughput dense coatings, the gun can also tailor the composition of the coating by introducing powder particles (e.g. carbide) through the HVOF jet, to cater to specific property requirements such as a functionally graded material (FGM). This paper presents the processing and microstructural evolution of a high performance iron alloy (nanosteel) coating developed by above mentioned hybrid-spray process. Further, coatings were also deposited by HVOF, plasma and twin wire arc-spray processes to compare their microstructure and properties with the hybrid-spray coatings. The specific alloy material selected here is a commercially available alloy with trade name nanosteel and it was originally developed for wear- and impact-resistant applications. The effect of the target preheating and temperature on the deposit quality and microstructures was investigated to develop adherent coatings.

2. Experimental Procedure

2.1 Precursor Material

Two precursors for nanosteel of similar compositions, cored wire, and powder feed stock, were employed depending on the spray process employed to develop the coatings. The composition for both the feedstock materials is shown in Table 1, and a slight variation in the composition, especially the amount of tungsten, between the powder and wire precursors could be noticed, which was because of higher amount of tungsten in the sheath of the cored wire (verified by Energy dispersive x-ray analysis also). Wire feedstock was employed in the hybrid- and arc-spray processes, whereas the powder precursor was used in the plasma and HVOF processes.
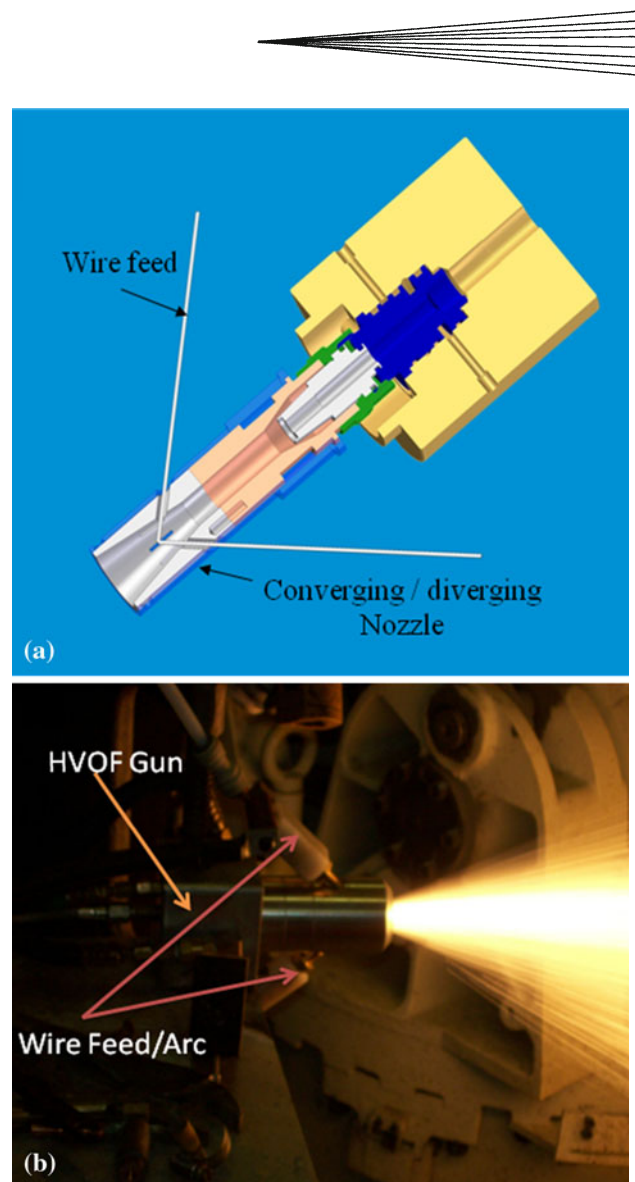

Fig. 1 (a) Schematic for hybrid-spray gun, (b) hybrid gun in operation

Table 1   Composition of feedstock materials

Weight, %	B	C	Cr	Fe	Mn	Mo	Si	W
Wire	5	2	26	51	4	4	3	5
Powder	5	2	20	51	5	5	2	10

2.2 Spray Processes

The above mentioned nanosteel coatings were-sprayed using HVOF-, plasma-, hybrid-, and arc-spray processes. HV-2000 System procured from Midwest Thermal Spray was used (Farmington Hills, MI) to spray HVOF coatings, and a mixture of propylene, oxygen, and air was used during the spray process. For plasma-spray process, Thermach AT 3000 Plasma System with a SG-100 gun was used. Arc-spray coatings were developed using TAFA 8830 Twin Wire Arc Spray System. Detailed description on the above three spray processes can be found

Table 2 Spray parameters

	Current	Voltage	Standoff distance, mm	Feed rate, g/min	Traverse speed, mm/s	Gas flow rate, standard liter per min
Plasma	600 A	32 V	75	30	300	Ar: 35
Arc	100 A	33 V	150	115	300	Air: 600
Hybrid	100 A	33 V	180	115	300	Fuel: 20 Oxy: 56 Air: 566
HVOF	…	…	205	30	300	Fuel: 20 Oxy: 56 Air: 566
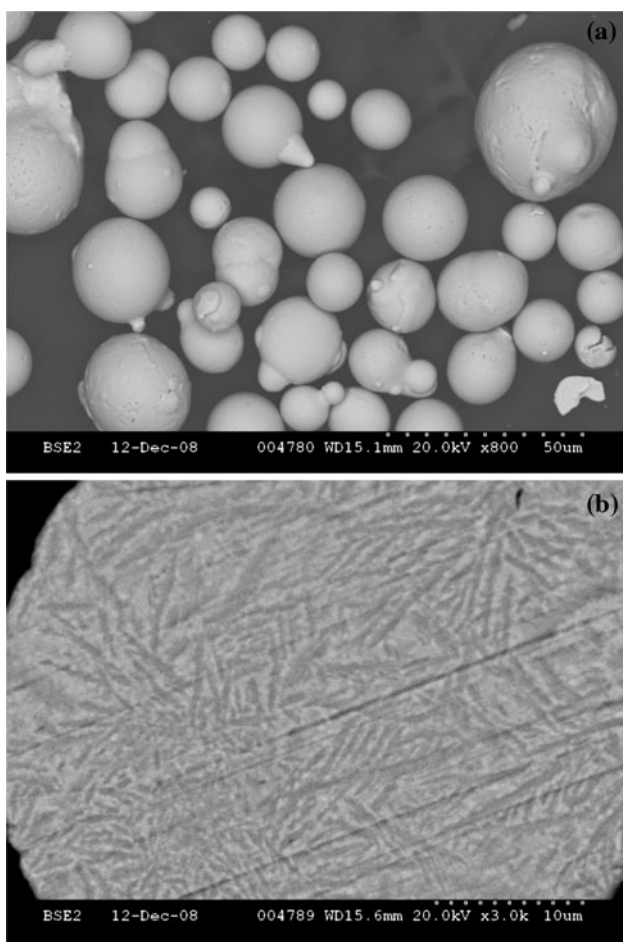
Fig. 2 SEM images of nanosteel powder precursor—(a) spherical powder particles with smooth morphology, and (b) BSE image of the powder particle

Fig. 3 SEM image of cored wire sheath with powder particles inside

elsewhere (Ref 25). A schematic for the fourth spray process, hybrid-spray technique, is shown in Fig. 1. The hybrid-spray configuration was designed and developed in our laboratory. This process combines the HVOF- and arc-spray processes. The HVOF component of the system combusts propylene/propane gases with oxygen and the gun is air cooled. The arc component is designed in such a way that the relative distance between the HVOF nozzle and the arc strike point, as well as the angle between the wires can be varied easily. Owing to flexible design, the hybrid gun can operate in three distinct modes: (i) partial-hybrid mo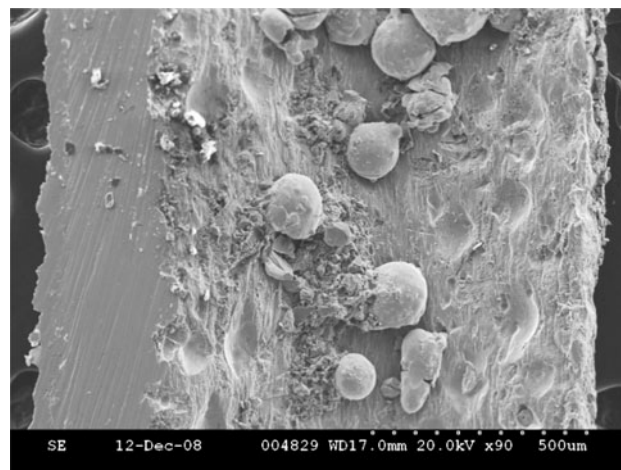de, where the material is introduced via arcing of wires only; the robustness of the hybrid gun allows it to be operated in two-wire arc or four-wire arc mode; (ii) fully hybrid mode, where the material is introduced through both arcing of wires and as a powder/ wire through the HVOF feed line, and this mode enables spraying of multiphase materials or embedding of a second phase in a matrix, and (iii) HVOF mode, where the material is fed into the HVOF gun in the form of powders or wire. More details on this system were reported elsewhere (Ref 24). A list of parameters used in all the spray processes is given in Table 2. In all the cases, coatings were sprayed with and without preheating of the steel substrates (1018 cold rolled steel, McMaster Carr., USA). Preheating was done using a PLC-controlled induction heater, and the preheating temperature was ~250 °C. To understand the effect of preheating and cooling processes on the evolution of microstructures, temperature profiles were recorded by placing a K-type thermocouple on the front face of the steel substrates.

2.3 Microstructure and Phase Evolution Characterization

All the coatings were analyzed using different analytical techniques. Initial characterization of as-sprayed coatings was done with a Hitachi S-2600N Scanning electron microscopy (SEM) to determine the quality of the coatings in terms of porosity and defects/cracks. Samples
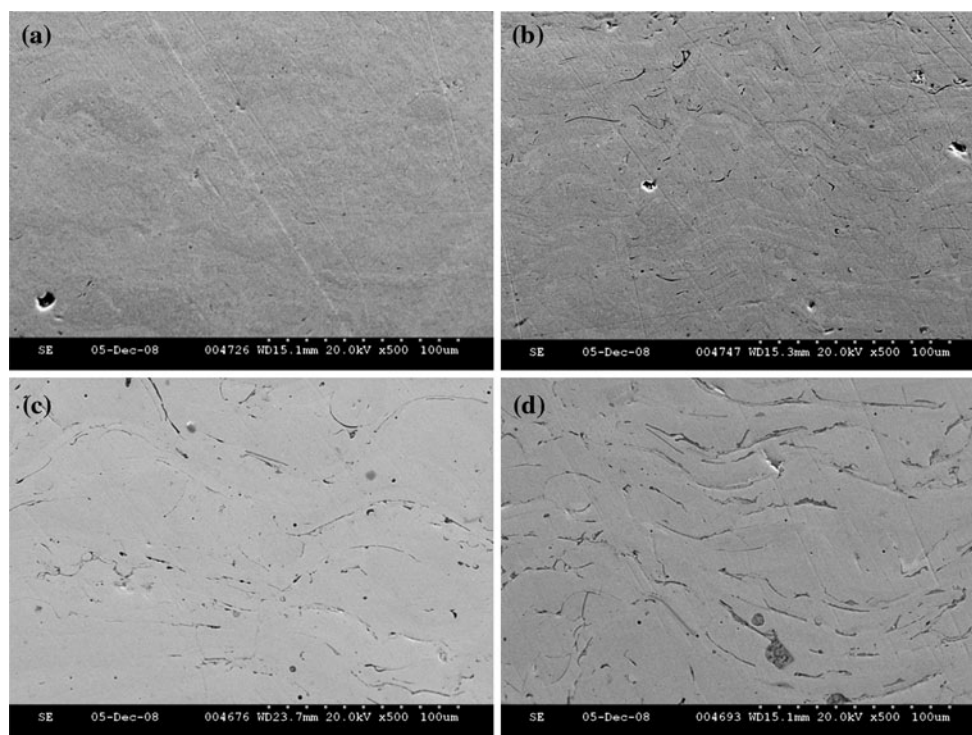
Fig. 4 Cross-sectional views of nanosteel coatings sprayed by (a) HVOF-, (b) plasma-, (c) hybrid-, and (d) arc-spray processes without preheating the substrate
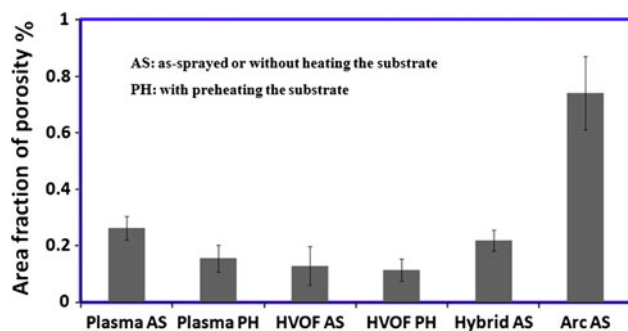

Fig. 5 Porosity of nanosteel coatings sprayed by different techniques with and without substrate preheating

for SEM studies were prepared following standard metallographic procedures. Compositions of the coatings were determined by means of Energy dispersive x-ray analysis (EDX) in SEM. Backscattered electron (BSE) imaging was also done to obtain composition contrast. For the phase analysis and crystallinity confirmation, x-ray diffraction (Rigaku MiniFlex, Cu K_α radiation with $\lambda = 1.5402°A$) and differential scanning calorimetry (DSC) (TA Instruments Q600 model) studies were conducted. DSC experiments were carried out in Ar atmosphere. Bulk microstructural characterization was done by Transmission electron microscopy (TEM) on a JEOL 2010F. The TEM samples were prepared by cutting 3-mm-diameter disks from the coatings after initial mechanical

thinning. To achieve electron beam transparency, final thinning was done using a Fischione twinjet Electropolisher model 110 at −25 °C, and the electropolishing agent was 5% $HClO_4 + 95\%$ CH_3OH solution.

2.4 Hardness Measurements

To assess the basic mechanical properties of the coatings, Vicker's hardness tests were done on a Future Tech FM1-E hardness tester with a 300-g load for a dwell time of 10 s.

3. Results and Discussion

3.1 Characterization of Precursors

SEM images of wire feed stock and powders of nanosteel are shown in Fig. 2 and 3. As-received powders have spherical shape (size ~30-50 μm) with smooth surface morphology (Fig. 2a). The microstructural analysis of powders reveal multiphase structure of the powders in BSE image shown in Fig. 2(b), and crystallinity was confirmed by x-ray diffraction studies, which will be discussed in the forthcoming section. The wire feedstock consisted of smooth spherical powder particles (size ~100-150 μm) inside a wire sheath as shown in Fig. 3. A considerable difference in the size of powder particles of the powder precursor and the cored wire precursor could be noticed.
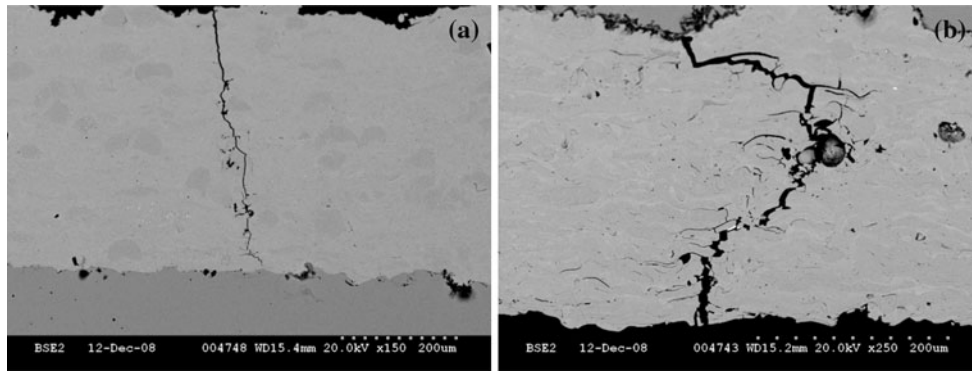
Fig. 6 BSE images of nanosteel coatings sprayed by (a) HVOF-, and (b) plasma-spray processes without substrate preheating. Through thickness cracks are visible in the HVOF- and plasma-spray coatings
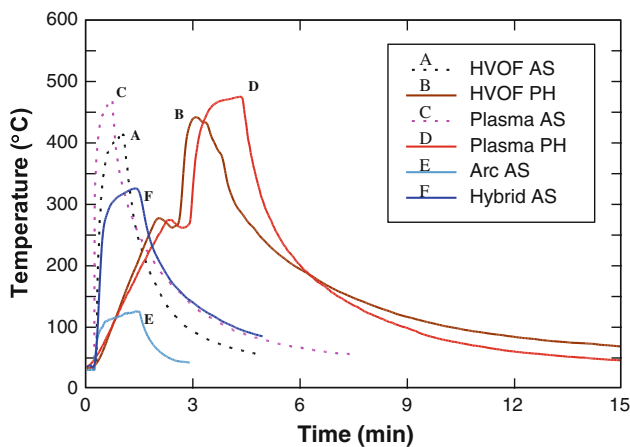

Fig. 7 Temperature profiles for the coatings sprayed by different techniques (with and without substrate preheating), which include the temperature measurements before, during, and after the spray process

Table 3 Cooling rates in different spray processes for a $\Delta t = 2$ min after the spray process

	°C/s
HVOF without preheating	2.67
HVOF with preheating	1.83
Plasma without preheating	2.76
Plasma with preheating	2.33
Arc without preheating	0.71
Hybrid without preheating	1.67

3.2 Observation of Coatings without Pre-heating the Substrate

Nanosteel coatings were initially sprayed without preheating the steel substrates using all the four spray processes. Figure 4 shows the SEM images of cross-sectional views of the coatings developed by HVOF-, plasma-, hybrid-, and arc-spray techniques. Porosity of the coatings was measured using Pax-IT software availing several SEM images. The amount of porosity measured in each case is

shown in Fig. 5. From the Fig. 4 and 5, it is clear that HVOF coatings are quite dense with minimal amount of porosity. The plasma- and hybrid-spray coatings have comparable porosity, and the arc-spray coatings have the highest porosity. Both the hybrid- and arc-spray techniques make use of arc component of the spray process to atomize the spray material; however, the presence of HVOF plume in the hybrid-spray technique increases the particle velocity and thus help in densification of the coatings. The plasma and HVOF coatings showed cracking in certain regions, which are shown in Fig. 6. On the other hand, hybrid- and arc-spray coatings showed no cracking except the splat boundaries, see Fig. 4(c) and (d). The cracks observed in the HVOF and plasma coatings could be attributed to possible rapid quenching of the deposited coatings. To confirm this, the temperatures and cooling rates of the substrates were measured during the spray process. Figure 7 shows the temperature profiles obtained in all the four spray techniques. Maximum substrate temperatures attained in the plasma and HVOF processes are higher compared with the hybrid- and arc-spray techniques, which could be attributed to high heat input plume temperatures in both the spray processes (Ref 25). In addition, the extensive lamellar structures of both the hybrid- and arc-spray coatings could provide room for relaxation of residual stresses.

The cooling rates are calculated using the following equation from the peak temperatures in each case:

$$\text{Cooling rate} = \frac{\Delta T}{\Delta t} \tag{Eq 1}$$

where ΔT is the amount of drop in temperature from the peak temperature in a given time period of Δt. Table 3 shows the cooling rates calculated for all the four spray techniques for a time period of $\Delta t = 2$ min at the end of the spray process. However, it should be clearly noted that the above cooling rates calculated based on Eq 1 depict only the extent of cooling or cooling rates of the coatings for comparison purposes in the respective coatings, but they do not accurately represent the cooling rates required for the formation of amorphous phases in the coatings as they are well below the actual glass transition temperature of this alloy (~540 °C). In addition, these measurements do
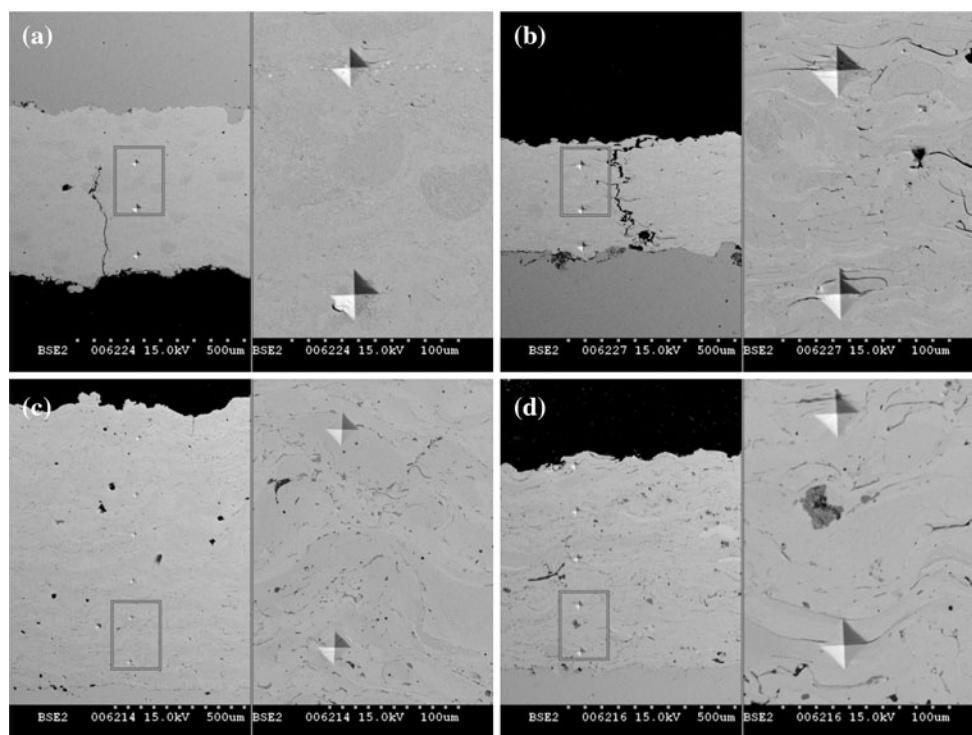
Fig. 8 Variation in the indentation sizes for (a) HVOF coating and (b) plasma coating compared with the consistent hardness indents in (c) hybrid- and (d) arc-spray coatings for a load of 300 g and 10 s dwell time
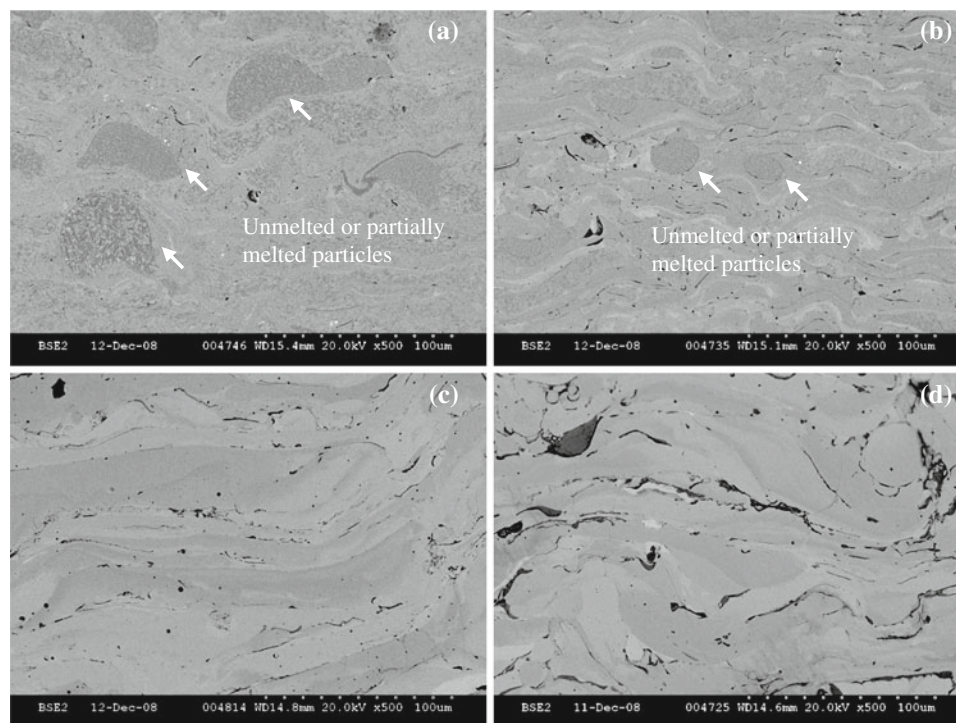

Fig. 9 SEM BSE images of nanosteel coatings sprayed by (a) HVOF-, (b) plasma-, (c) hybrid-, and (d) arc-spray processes without preheating the substrate

not indicate the real dynamic situation of thermal history in the substrates and coatings accurately. From Fig. 7 and Table 3, it is evident that the temperature drops are steeper in the plasma and HVOF processes compared with the arc and hybrid techniques, which is an indication for rapid quenching of the substrates upon completion of the

spray processes. Consequently, the amount of residual thermal stresses expected in the HVOF- and plasma-spray coatings is also large, which can eventually lead to cracking of the coatings.

Besides the above observations, HVOF and plasma coatings showed a very nonuniform hardness compared with the hybrid- and arc-spray coatings. The size of the indents varied across the HVOF and plasma coatings for a constant load. Variation in the indent size in the HVOF and plasma coatings is shown in Fig. 8. Changes of indentation sizes in the HVOF- and plasma-spray coatings could be either due to possible variation in the local composition or because of partially melted feedstock material in the coatings. To verify this, phase contrast imaging was done using back scattered electron imaging (BSE) in the SEM. Figure 9 shows the BSE images of HVOF-, plasma-, hybrid- and arc-spray techniques. It is apparent that there is a considerable variation in the phase contrast in the arc-spray coatings compared with the other
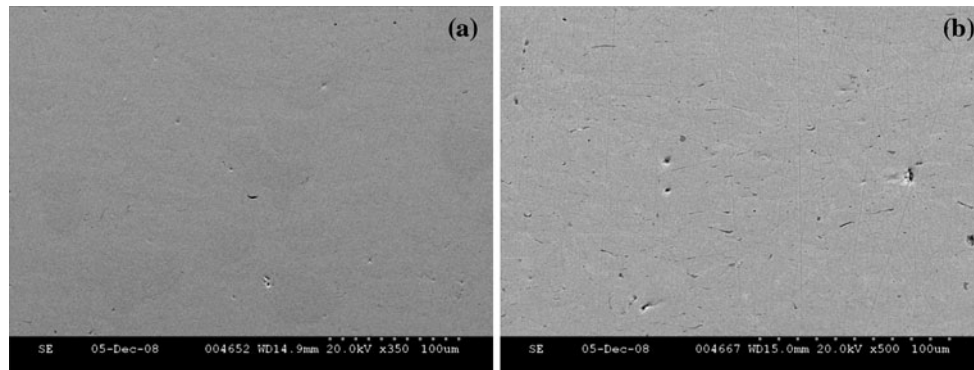
Table 4 Vicker's hardness data

HVOF with preheating	1189 ± 90.7
Plasma with preheating	1629 ± 96.4
Hybrid without preheating	1142.3 ± 59.4
Arc without preheating	939.7 ± 47.5

Fig. 10 SEM images of nanosteel coatings sprayed by (a) HVOF- and (b) plasma-spray processes with preheating the substrates to 250 °C
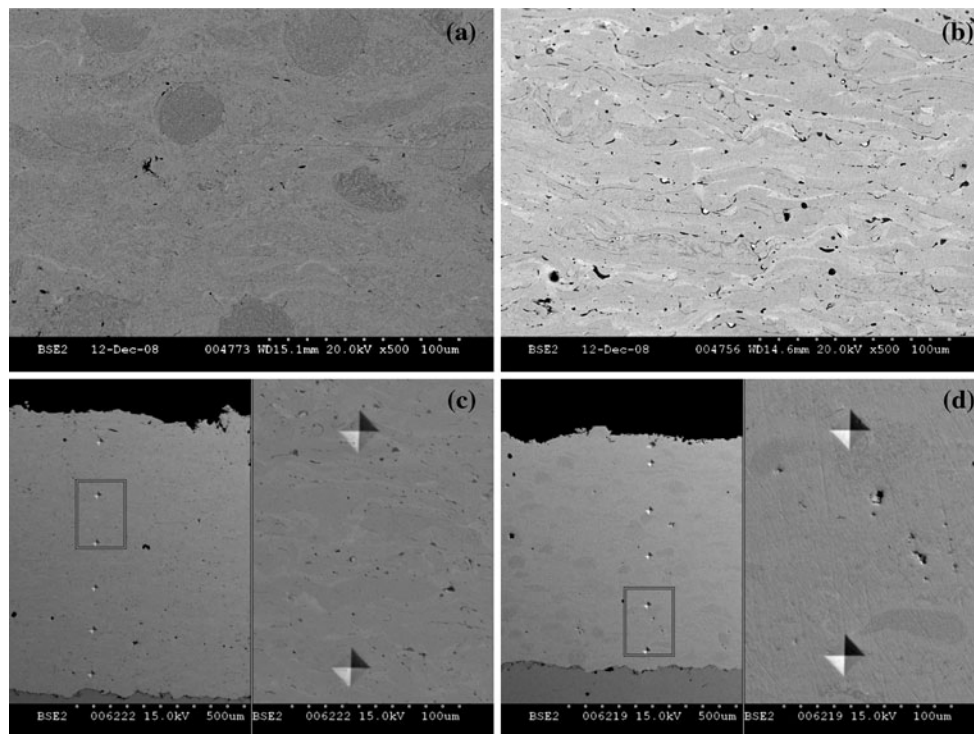

Fig. 11 SEM BSE images of nanosteel coatings sprayed by (a) HVOF, (b) plasma-spray processes and consistent indentation of Vicker's indenter without cracking in (c) HVOF and (d) plasma coatings after preheating the substrates
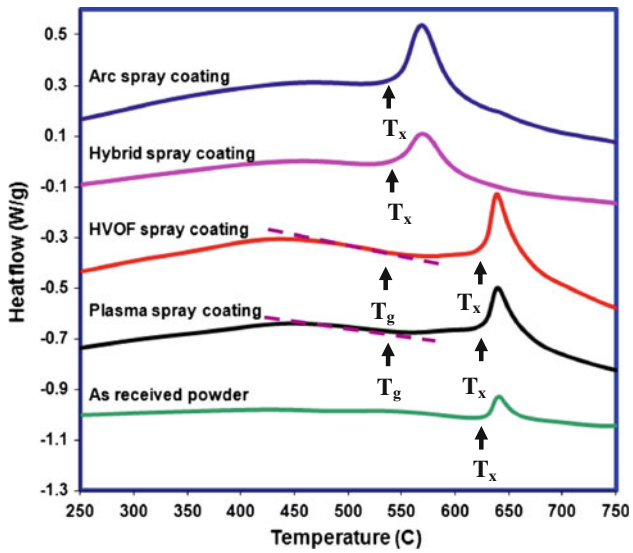
Fig. 12 DSC curves for different coatings: HVOF—preheated, plasma—preheated, hybrid—without preheating, arc—without preheating, and as-received nanosteel powder feedstock

Fig. 13 x-ray diffraction patterns for different coatings: HVOF—preheated, plasma—preheated, hybrid—without preheating, arc—without preheating, and as-received nanosteel powder feedstock
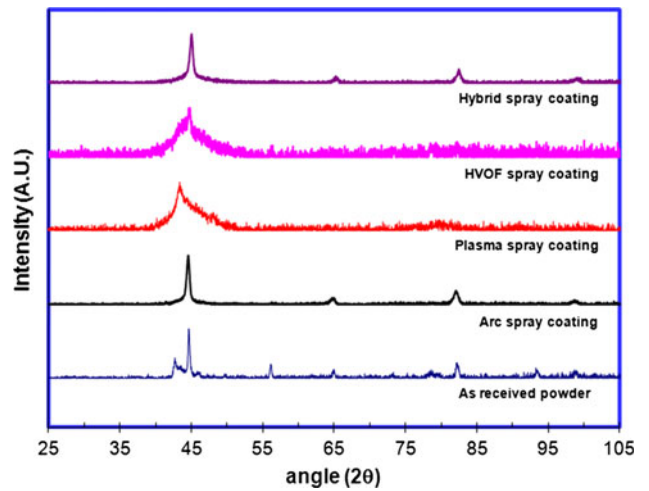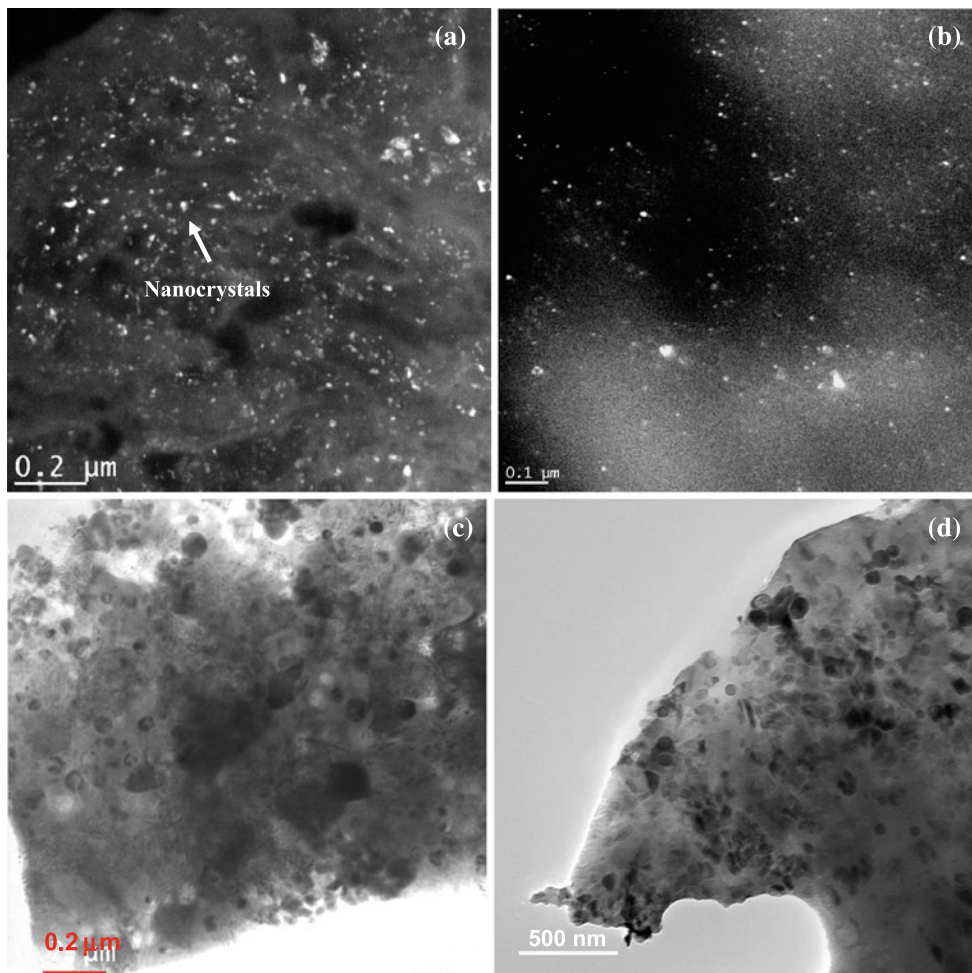

Fig. 14 Dark field TEM images of nanosteel coatings developed by (a) HVOF- and (b) plasma-spray processes, and bright field TEM images of nanosteel coatings developed by (c) hybrid and (d) arc techniques
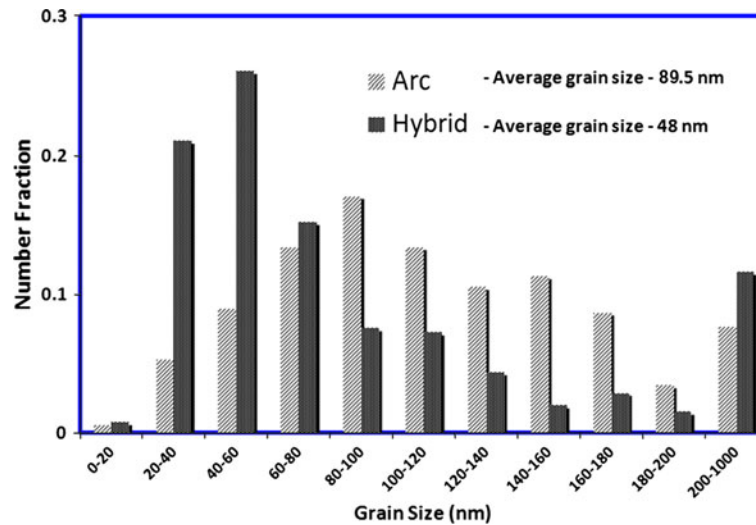
Fig. 15 Grain size distributions for nanosteel coatings developed by arc- and hybrid-spray techniques

three coatings, but there is no unmelted feedstock. However, the presence of HVOF plume in the hybrid-spray technique improved the overall quality of coatings by increasing the process temperature and atomization, thereby minimized the phase segregation compared with the arc-spray coatings. On the other hand, HVOF and plasma coatings have a very minimal variation in the composition, but there are few unmelted or partially melted feedstock powder particles clearly visible. In spite of chemical segregation, the arc-spray coatings did not show much variation in the indent size. Therefore, variation in the hardness indent size on the HVOF and plasma coatings could be due to unmelted or partially melted feedstock. Usually, high velocity of feed stock along with short dwell time in the HVOF and plasma plumes could lead to partial melting, if the feed particles are above certain size. This may induce differential cooling rates in the coatings upon striking the substrate and thereby vary the thermal residual stresses between the completely and partially melted feedstock. This could also be one of the reasons why the HVOF and plasma coatings showed cracking in the as-sprayed condition.

3.3 Physical Observation of Coatings with Preheating of Substrates

From the application point of view, cracks and inconsistent mechanical properties can lead to poor performance of the coatings. This being the main goal; further studies were focused on improving the quality of the coatings by preheating the substrates to reduce the cooling rates. However, the spray parameters were kept constant in all the cases.

After several iterations of preheating the substrates to various temperatures, HVOF and plasma coatings were observed to perform better in terms of uniform hardness (see Table 4) without cracking when the substrates were preheated to 250-270 °C. On the other hand, preheating of substrates in the hybrid- and arc-spray processes did not result in any improvement of the coatings.

Figure 10 shows the cross sectional view of the coatings sprayed by HVOF and plasma techniques while preheating the substrates to 250 °C for a period of 5 min. The porosity measurements shown in the Fig. 5 indicate the extent of densification that was achieved in the HVOF and plasma coatings while preheating the substrates. In addition, HVOF- and plasma-spray coatings exhibited uniform hardness without any cracking, see Table 4. The hardness data shown in the Table 4 was obtained from a total of 10 measurements in each case. Figure 11 shows the phase contrast SEM images of HVOF and plasma coatings with preheated substrate. The HVOF coating has partially melted or unmelted feed stock, whereas plasma coating shows a considerable variation in the phase contrast. The temperature profiles for the preheated substrate-coating systems in the HVOF- and plasma-spray processes are shown in the Fig. 7. The cooling rate data from Table 3 indicates a significant decrease in the cooling rates in the HVOF- and plasma-spray processes due to preheating of the substrate-coating systems, which could reduce the amount of residual stresses in the coatings compared with the as-sprayed condition without preheating the substrate-coating systems. From the Table 3 it is also apparent that the cooling rates in HVOF- and plasma-spray techniques with preheating are similar to the hybrid-spray technique.

From the above observations, we conclude that preheating is desired only in the HVOF- and plasma-spray techniques compared to the hybrid- and arc-spray techniques. Temperatures and velocities achieved in the hybrid-spray technique may not quench the coatings as rapidly as they do in other spray processes and thereby help in reducing the porosity to maintain the structural integrity without cracking. Thus developed nanosteel coatings with optimized conditions in all the processes were considered for further investigation to study the
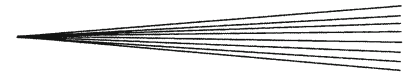
microstructures as well as to understand the effect of spray process employed.

3.4 Phase and Microstructural Characterization of Coatings

Phase characterization, crystallinity, and grain size determination of the optimized nanosteel coatings were done by DSC analysis, x-ray diffraction (XRD), and TEM studies, respectively. DSC curves for all the coatings are shown in Fig. 12. Endothermic steps in the HVOF and plasma coatings indicate the presence of amorphous phase. The glass transition temperature (T_g) of these coatings is ~540 °C. DSC heat flow curves for the arc and hybrid coatings do not show any endothermic step, and this could be either because of the absence of amorphous structure or lower amorphous content levels that could be below the detection sensitivity of the DSC machine. However, in all the cases exothermic recrystallization peaks (T_x) are clearly visible. The different T_x values between the arc/hybrid coatings and the HVOF/plasma coatings are due to the feedstock materials employed. Since the powder feedstock was used in both the HVOF and plasma techniques, the T_x values for feedstock powder and the coatings do match very well.

From the XRD patterns, which are shown in Fig. 13, it is evident that the coatings produced by HVOF- and plasma-spray processes may possibly have amorphous structure because of a broad peak, whereas the hybrid- and arc-spray coatings show prominent polycrystalline peaks. The XRD pattern of as-received powder feedstock indicates polycrystalline structure. Amorphous structures usually form when the cooling rates are high enough to hinder the crystallization kinetics. As discussed earlier, steep temperature drops in the HVOF and plasma techniques could indicate likelihood of formation of the amorphous structures in the coatings, although the data shown in Table 3 do not necessarily represent the cooling rates required for the formation of amorphous structures. On the other hand, slow cooling rates and low process temperatures lead to crystallization of molten splats in the hybrid- and arc-spray coatings. In addition, large powder particle size and cored wire sheath could lead to bigger splat sizes in the hybrid- and arc-spray processes compared with the splat sizes in the plasma and HVOF techniques, where powder precursor was employed. Therefore, slow quenching of splats in the hybrid- and arc-spray techniques could end up in easy crystallization and polycrystalline coatings.

The absence of crystalline peaks in the HVOF and plasma coatings due to the partially melted feedstock may be attributed to limited depth of penetration of the x-rays during the XRD scans as most of the unmelted or partially melted feedstock was embedded in the bulk of the coatings. The XRD patterns for hybrid- and arc-spray coatings show only Fe/steel peaks, which is the base material (see the chemical composition Table 1), with considerable peak broadening. The absence of the XRD peaks for other elements could be attributed to formation of nanosteel alloy in the coatings. Further microstructural analysis

was carried out by TEM to investigate the existence of amorphous and nanocrystalline structures in all the coatings, and the grain size measurements were done following line intercept method.

TEM images for all the four coatings are shown in Fig. 14. Dark field images captured using (110) diffraction ring for the plasma and HVOF coatings show fine nanocrystals in the amorphous matrix. The absence of crystalline peaks in the XRD measurements could be due to small weight fraction of the nanocrystals in the plasma and HVOF coatings. On the other hand, arc and hybrid coatings revealed a bi-modal microstructure with fine and coarse nano grains. Figure 15 shows the grain size distribution and average grain size in both the arc and hybrid coatings. The large grain size in hybrid-spray coatings could be due to the processing temperatures and standoff distance employed, which could control the extent of quenching and thus crystallization of the coatings.

Based on the microstructures, we conclude that the HVOF and plasma coatings were cracking because of amorphous matrix and residual stresses, as cooling rates were very high in these techniques. However, bi-modal microstructure in the arc and hybrid coatings revealed to be a better choice from the coating quality point of view as they show uniform hardness in spite of compositional variation. Nevertheless, the hybrid coatings have enhanced density with better hardness compared to the arc-sprayed coatings. Thus, the nanosteel coatings developed by hybrid-spray technique have optimized quality in terms of porosity, uniform hardness, and microstructure compared with the coatings developed by other three spray processes.

4. Conclusions

The effect of different spray processes and spray parameters on the microstructural evolution and coating qualities was investigated systematically. HVOF and plasma techniques being powder-based processes with rapid cooling rates in the coatings may require preheating to avoid cracking in the coatings as well as to obtain uniform mechanical properties. The hybrid and arc are robust techniques that require minimal efforts to obtain the coatings without any cracking in the as sprayed condition; however, the hybrid technique with moderate process temperatures and quench rates is superior to the arc-spray process to obtain better quality coatings in terms of porosity and uniform phase segregation. The microstructural evolution indicates that plasma and HVOF techniques lead to amorphous structures with very little crystallization due to rapid cooling rates; on the other hand, hybrid- and arc-spray techniques provide bi-modal nanocrystalline structure with improved properties. Further characterization of these coatings in terms of wear, corrosion, and erosion performance along with the mechanical properties will be reported in the subsequent publications.

References

1. J. Musil, Hard and Superhard Nanocomposite Coatings, *Surf. Coat. Tech.*, 2000, **125**(1–3), p 322-330
2. S. Zhang, D. Sun, Y. Fu, and H. Du, Recent Advances of Superhard Nanocomposite Coatings, *Int. Conf. Mater. Process. Prop. Perf. (MP3)*, 2003, **167**(2–3), p 113-119
3. S. Veprek and S. Reiprich, A Concept for the Design of Novel Superhard Coatings, *Thin Solid Films*, 1995, **268**(1–2), p 64-71
4. S. Veprek, M. Haussmann, S. Reiprich, and Li. Shizhi, Novel Thermodynamically Stable and Oxidation Resistant Superhard Coating Materials, *J. Dian: Surf. Coat. Tech.*, 1996, **86–87**, p 394-401
5. A. Inoue, *Bulk Amorphous Alloys: Preparation and Fundamental Characteristics*, Trans. Tech. Pub, Zurich, 1998
6. D. Neerinck, P. Persoone, M. Sercu, A. Goel, D. Kester, and D. Bray, Diamond-like Nanocomposite Coatings (aC: H/a-Si: O) for Tribological Applications, *Diam. Relat. Mater.*, 1998, **7**(2–5), p 468-471
7. S. Veprek, A. Niederhofer, K. Moto, T. Bolom, H.-D. Mannling, P. Nesladek, G. Dollinger, and A. Bergmaier, Composition, Nanostructure and Origin of the Ultrahardness in nc-TiN/a-Si$_3$N$_4$/a- and nc-TiSi$_2$ Nanocomposites with H_V=80 to ≥105 GPa, *Surf. Coat. Tech.*, 2000, **133–134**, p 152-159
8. J. Musil, P. Karvankova, and J. Kasl, Hard and Superhard Zr–Ni–N Nanocomposite Films, *Surf. Coat. Tech.*, 2001, **139**(1), p 101-109
9. D.J. Branagan, Developing Extreme Hardness (>15 GPa) in Iron Based Nanocomposites, *Yali Tang Compos. PartA Appl. S.*, 2002, **33**(6), p 855-859
10. A.A. Voevodin, J.P. O'Neill, and J.S. Zabinski, Nanocomposite Tribological Coatings for Aerospace Applications, *Surf. Coat. Tech.*, 1999, **116--119**, p 36-45
11. S. Carvalho, E. Ribeiro, L. Rebouta, C. Tavares, J.P. Mendonca, A. Caetano Monteiro, N.J.M. Carvalho, J.Th.M. De Hosson, and A. Cavaleiro, Microstructure, Mechanical Properties and Cutting Performance of Superhard (Ti,Si,Al)N Nanocomposite Films Grown by d.c. Reactive Magnetron Sputtering, *Surf. Coat. Tech.*, 2004, **177--178**, p 459-468
12. J. He and J.M. Schoenung, Nanostructured Coat, *Mater. Sci. Eng. A*, 2002, **336**(1–2), p 274-319
13. D.J. Branagan, Enabling Factors Toward Production of Nano-structured Steel on an Industrial Scale, *J. Mater. Eng. Perform.*, 2005, **14**(1), p 5-9
14. J. Colmenares, M. Rodriguez, and A. Scagni, Optimization of Thermally Sprayed Metallic Nanocomposite Coatings, *3rd International Surface Engineering Congress*, 2005, p 114-119
15. D.A. Stewart, P.H. Shipway, and D.G. McCartney, Microstructural Evolution in Thermally Sprayed WC–Co Coatings: Comparison Between Nanocomposite and Conventional Starting Powders, *Acta Mater.*, 2000, **48**(7), p 1593-1604
16. M.L. Lau, V.V. Gupta, and E.J. Lavernia, Particle Behavior of Nanocrystalline 316-Stainless Steel During High Velocity Oxy-Fuel Thermal Spray, *Nano. Mater.*, 1999, **12**(1–4), p 319-322
17. D. J. Branagan, M. C. Marshall, and B.E. Meacham, Development of Highly Wear Resistant Iron Based PTAW Hardfacing Alloys, *Proceedings of International Thermal Spray Conference (ITSC)*, 2005, p 539–544
18. M. Cherigui, H.I. Feraoun, N.E. Feninehe, H. Aourag, and C. Coddet, Structure of Amorphous Iron-Based Coatings Processed by HVOF and APS Thermally Spraying, *Mater. Chem. Phys.*, 2004, **85**(1), p 113-119
19. K. Kishitake, H. Era, and F. Otsubo, Characterization of Plasma Sprayed Fe-17Cr-38Mo-4C Amorphous Coatings Crystallizing at Extremely High Temperature, *J. Therm. Spray. Techn.*, 1996, **5**(4), p 476-482
20. D.J. Branagan, M. Breitsameter, B.E. Meacham, and V. Belashchenko, High-Performance Nanoscale Composite Coatings for Boiler Applications, *J. Therm. Spray Techn.*, 2005, **14**(2), p 196-204
21. D.J. Branagan, W.D. Swank, D.C. Haggard, and J.R. Fincke, Wear-Resistant Amorphous and Nanocomposite Steel Coatings, *Metall. Mater. Trans. A*, 2001, **32A**(10), p 2615-2621
22. D. Kosikowski, M. Batalov, and P.S. Mohanty, Functionally Graded Coatings by HVOF-Arc Hybrid Spray Gun, *Proceedings of International Thermal Spray Conference (ITSC05)*, 2005, p 444-449
23. D. Kosikowski, M. Batalov, and P. Mohanty, In-Flight Particle Characterization of HVOF-Arc Hybrid Gun, *Proceedings of International Thermal Spray Conference (ITSC05)*, 2005, p 785-790
24. J. Stanisic, D. Kosikowski, and P.S. Mohanty, High-Speed Visualization and Plume Characterization of the Hybrid Spray Process, *J. Therm. Spray Techn.*, 2006, **15**(4), p 750-758
25. L. Pawlowski, *The Science and Engineering of Thermal Spray Coatings*, 2nd ed., Wiley, West Sussex, 2008, p 180-190